Ocean Engineering 187 (2019) 106210

Contents lists available at ScienceDirect

Ocean Engineering

journal homepage: www.elsevier.com/locate/oceaneng

Short communication

On the relaxation approach for wave absorption in numerical wave tanks

Qiang Chen [a], David M. Kelly [b], Jun Zang [a,*]

[a] Research Unit for Water, Environment and Infrastructure Resilience (WEIR), Department of Architecture and Civil Engineering, University of Bath, BA2 7AY, UK
[b] Department of Mechanical and Materials Engineering, Florida International University, Miami, FL, 33199, USA

ARTICLE INFO

Keywords:
Numerical wave tank
Wave absorption
Relaxation method
Particle-In-Cell method

ABSTRACT

In CFD modelling, relaxation methods are widely used in numerical wave tanks (NWTs) for wave absorption; however, this method can be very expensive as part of the NWT must be dedicated to a relaxation zone. In this short technical note, a parametric study on the effects of the relaxation approach on absorbing different types of waves is reported. In addition, a simple modification to the relaxation method is suggested. The results appear to show that the modified relaxation approach helps to reduce the length of the relaxation zone by nearly half whilst retaining good performance in terms of wave absorption.

1. Introduction

Numerical wave tanks (NWTs) are widely used in computational fluid dynamics (CFD) modelling in the coastal and offshore engineering field. Typically, waves are generated at one end of the NWT and absorbed at the other end so that the desired waves can be produced within the focus section of the NWT. Numerical techniques for wave absorption may be categorised as active methods and passive methods; while active methods refer to those modifying the computational results in a zone or boundary of the NWT, passive methods represent those implementing a slope in the NWT to resemble physical beaches (Windt et al., 2018). Typical examples in the active wave absorption category are relaxation methods (Jacobsen et al., 2012), static/dynamic boundary methods (Higuera et al., 2013; Armesto et al., 2014) and numerical beach implementation (Koo and Kim, 2004), and, as mentioned above, a typical example in the passive wave absorption category is the sloping beach method (Finnegan and Goggins, 2012). For a comprehensive review of numerical wave absorption techniques, the reader is referred to Windt et al. (2018).

The relaxation method is one of the most popular wave absorption techniques (Mayer et al., 1998; Madsen et al., 2003; Engsig-Karup et al., 2006; Fuhrman et al., 2006; Jacobsen et al., 2012; Kamath et al., 2015; Chen et al., 2018), as it is straightforward and flexible to implement and also because this method has been successfully implemented in the waves2Foam toolbox for the open-source CFD library OpenFOAM®(Jacobsen et al., 2012). The idea being that in a region of the NWT (usually at the downstream end) that is referred to as relaxation zone, the numerical solution is gradually relaxed by:

$$\boldsymbol{\phi} = \xi \boldsymbol{\phi}_{\text{computed}}, \tag{1}$$

where $\boldsymbol{\phi}$ represents a fluid quantity (e.g. velocity) and ξ is a relaxation function which is 1 at the interface where the relaxation zone starts and gradually changes to 0 at the end of the relaxation zone. The performance of the relaxation method thus depends on the length of the relaxation zone and the variation of the relaxation function, which are very likely to be interrelated. Engsig-Karup (2006) discussed the form of the relaxation function based on discontinuous Galerkin methods and suggested that the relaxation function has to fulfil the conditions that $\xi = 1$ and $\xi' = \xi'' = \xi''' = \cdots = 0$ at the starting interface of the relaxation zone. This indicates that an ideal relaxation function should be perfectly flat at the starting interface. In practice, however, these conditions only need to be fulfilled to a certain degree.

One of the most widely employed relaxation functions is that proposed in Fuhrman et al. (2006) (see e.g. Jacobsen et al. (2012), Paulsen et al. (2014), Chen et al. (2016a, 2018), Palm et al. (2016, 2018)):

$$\xi(x_p) = 1 - \frac{\exp(x_r^{3.5}) - 1}{\exp(1) - 1}, \tag{2}$$

where $x_r = (x_p - x_{\text{start}})/L_I$, and x_p, x_{start} and L_I are a location inside the relaxation zone, the starting interface of the relaxation zone and the length of the relaxation zone, respectively. To achieve a cost-effective performance using this relaxation function, a length of 1 – 4 wavelengths is usually employed for the relaxation zone (see e.g. Chen et al. (2016a, 2018), Palm et al. (2016, 2018)). Other types of relaxation functions are mostly based on polynomials of high degree (Mayer et al., 1998; Engsig-Karup et al., 2006; Kamath et al., 2015), which have similar profiles to that of Eq. (2). In addition, as a rule of thumb, a relaxation zone of approximately two wavelengths long is needed for these polynomial based relaxation functions. Therefore, a disadvantage of the

* Corresponding author.
E-mail addresses: chenqiang913@hotmail.com (Q. Chen), dakelly@fiu.edu (D.M. Kelly), j.zang@bath.ac.uk (J. Zang).

https://doi.org/10.1016/j.oceaneng.2019.106210
Received 17 January 2019; Received in revised form 2 May 2019; Accepted 6 July 2019
Available online 12 July 2019

relaxation method for wave absorption is that a part of the NWT must be dedicated to the relaxation zone. This makes the relaxation method particularly expensive when the wavelength is large (see e.g. Palm et al. (2016), Ransley et al. (2017), Chen et al. (2019)).

In this short note, the relaxation function shown in Eq. (2) is further examined and tested for wave absorption on different types of waves. In addition, based on the examinations a straightforward technique is proposed to modify conventional relaxation approaches. The modified relaxation approach appears to reduce the length of the relaxation zone by nearly half (compared to a normally used length) whilst still maintaining overall good performance of wave absorption.

The computations presented in this short note employ the Particle-In-Cell (PIC) method based model proposed in Chen et al. (2016b) (2D version) and Chen et al. (2018) (3D parallel version). The PIC model utilises both an Eulerian grid and a set of Lagrangian particles to solve the incompressible Navier–Stokes equations for free-surface flows. The hybrid particle-grid nature makes the model both efficient (in terms of CPU cost) and flexible when solving complex physical problems involving large free-surface deformations. The NWT established within the PIC model can handle wave generation/absorption and wave-structure interaction (via a Cartesian cut cell method). For full details of the development of the current PIC method based CFD model, the reader is also referred to Kelly et al. (2015), Chen et al. (2016a, 2019). In addition, for a review of the development history of the PIC method, the reader is referred to Harlow (2004), Edwards (2015), Chen (2017).

2. Relaxation approach and a modification

Fig. 1 shows a typical free-surface profile of a regular wave propagating into a relaxation zone implemented at the downstream end of a 2D NWT. The computation employs the PIC model that solves the incompressible Newtonian Navier–Stokes equations for free-surface flows (Chen et al., 2016b; Chen, 2017). The wave has reached a steady state. The length of the relaxation zone is set to $2.25L$ (L is the wavelength), and Eqs. (1) and (2) are employed to dissipate the fluid velocity only (i.e. $\boldsymbol{u} = \xi \boldsymbol{u}_{\text{computed}}$). It can be observed that as the regular wave propagates into the relaxation zone (starting with $x_r = 0$) the wave height is gradually reduced as expected. However, it is interesting to note that the majority of the wave energy is dissipated in the front half of the relaxation zone ($0 \leq x_r \leq 0.5$), and in the back half of the relaxation zone ($0.5 < x_r \leq 1.0$) the free surface remains almost still. This may lead us to two conclusions: (1) the wave is mainly absorbed in the flat portion of the relaxation function ($\xi \sim 1.0$), and (2) the steep changing portion of the relaxation function (i.e. $0.5 < x_r \leq 1.0$) is not overly critical and can be removed to reduce the size of the computational domain and hence the CPU effort expended. To explain the first point, the details of the numerical simulation are examined. In the case presented here, the non-dimensional wave period $T\sqrt{g/h}$ (T is the wave period, g is the gravitational acceleration and h is the water depth) is 5.6, and the average time step $\Delta t\sqrt{g/h}$ is 0.029. So, by the time the wave has propagated half the relaxation zone length (namely $1.125L$), the fluid velocity has been dissipated $5.6/0.029 \times 1.125 \approx 217$ times (note that Eq. (1) is applied at every time step). Therefore, the corresponding wave energy has been dissipated by an amount of approximately $(\xi^{217})^2$. As a rough guide, if ξ is given a constant value 0.9954, which is the value at the location of a quarter of the relaxation zone length (i.e. $x_r = 0.25$), the wave energy has been dissipated to nearly 13.5% of its value at the beginning of the relaxation zone. This explains the first point raised above and suggests that the second point is also valid.

Based on the above findings, a modified relaxation method for efficient wave absorption in NWTs is now proposed, which aims to use nearly half the resource of a regular relaxation method whilst achieving very similar performance. The idea is a simple one: to keep the flat portion of the relaxation function while removing the steep changing portion as seen in Fig. 1. Fig. 2 shows a schematic demonstrating the setup of the modified method; recalling Eq. (2), L_I is now referred to as an "imaged" or "input" relaxation zone length, while the length of the real relaxation zone required in the computational domain is denoted by L_R. Note that within the real relaxation zone, it is still the "imaged" or "input" relaxation length L_I that is used in the calculation of Eq. (2). In such a way, the real relaxation zone uses only the most-effective flat portion of the relaxation function and is *much* shorter than the length a regular relaxation method has to implement in the computational domain (i.e. L_I).

In the following section, the performance of the relaxation approach and the modified one are tested for wave absorption on different types of waves, considering also the effects of wave steepness and relaxation zone length. In addition, for the modified relaxation approach, effects of the ratio between L_R and L_I are reported.

3. Results and discussions

In this section, parametric studies are conducted to test the performance of the relaxation method and the modified version for absorbing three different type of waves: regular wave, solitary wave and focused wave. The computation uses the hybrid Eulerian–Lagrangian PIC solver developed by Chen et al. (2016b) and Chen et al. (2018), and both 2D and 3D NWTs are established following the same works according to the test cases under consideration. As in Section 2, Eq. (1) and Eq. (2) are used to dissipate the fluid velocity carried by the fluid particles that have entered the relaxation zone.

3.1. Regular wave tests

Fig. 3 shows the setup of a 2D NWT for the regular wave tests. Regular waves are generated upstream using a piston-type wave paddle and absorbed at the downstream end of the NWT employing the modified relaxation method. For all of the simulations, kh was fixed at 1.416, where k represents the wave number and h is the water depth. Three different wave steepnesses are tested: (a) $kA = 0.071$, (b) $kA = 0.106$, and (c) $kA = 0.142$, representing an increase in the nonlinearity of the incident waves. A uniform grid is used for all of the simulations with the grid size being $\Delta x = \Delta z \approx L/355$, where L is the wavelength. The Courant number is fixed at 0.5. In addition to the wave steepness, three different "imaged" relaxation zone lengths: (a) $L_I = 1.69L$, (b) $L_I = 2.25L$ and (c) $L_I = 2.82L$ are tested. The performance of the modified relaxation method is assessed by the reflection coefficient. Two wave gauges (WG2 and WG3, see Fig. 3) placed just in front of the relaxation zone are used for the calculation of the reflection coefficient using the two-point method proposed in Goda and Suzuki (1976).

3.1.1. Wave steepness

The reflection coefficients run with three different wave steepnesses are given in Table 1. Note that in these test cases the "imaged" relaxation zone length is $L_I = 2.25L$. The ratio of the real relaxation zone length L_R and the "imaged" relaxation zone length L_I ranges from 0.125 to 1.0. Note that when $L_R/L_I = 1.0$, the modified relaxation method is equivalent to the regular relaxation method.

First of all, it can be seen from Table 1 that in general for all of the three wave steepnesses the reflection coefficient decreases (as expected) from approximately 1.0 to 0.01 as the ratio L_R/L_I increases. Then, we focus on the reflection coefficients at the range $L_R/L_I = 0.5$ to 1.0. It is seen that for $kA = 0.106$, the reflection coefficient at $L_R/L_I = 0.5$ is almost the same as that at $L_R/L_I = 1.0$. This proves that at this test condition the modified relaxation method works as efficiently as the regular relaxation method, using however only half the relaxation zone length. For the sake of clarity, from hereafter we define the ratio L_R/L_I at which the modified relaxation method performs the same as the regular relaxation method as the "optimal ratio". For example, the optimal ratio for $kA = 0.106$ is approximately 0.5. For $kA = 0.071$ and 0.142, the stories are slightly different in reference to $kA = 0.106$. While

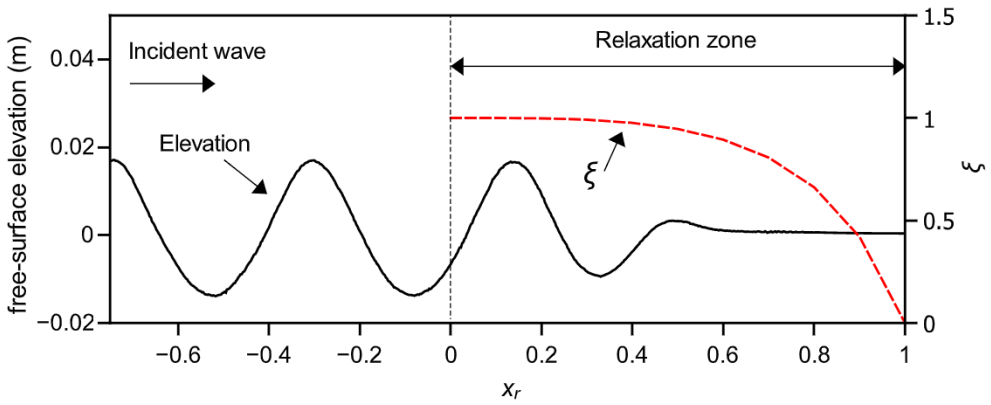

Fig. 1. A typical free-surface profile of regular wave propagating into a relaxation zone. The relaxation function ξ (see Eq. (2)) is plotted as the red dashed line.

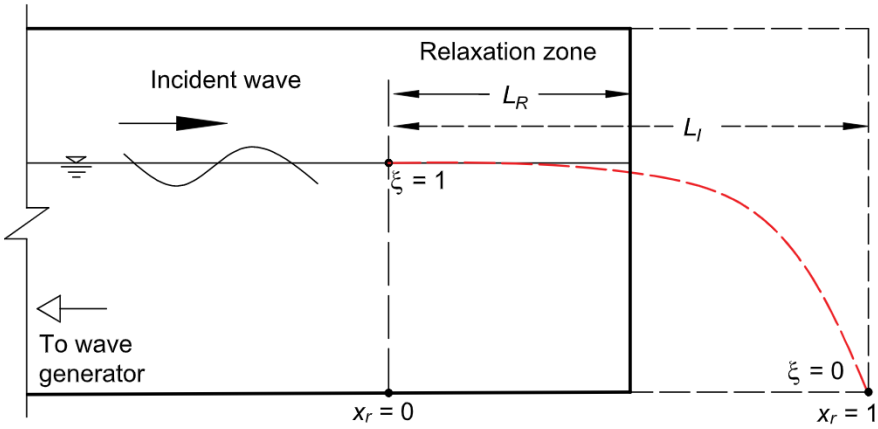

Fig. 2. Schematic showing the setup of the modified relaxation method for wave absorption.

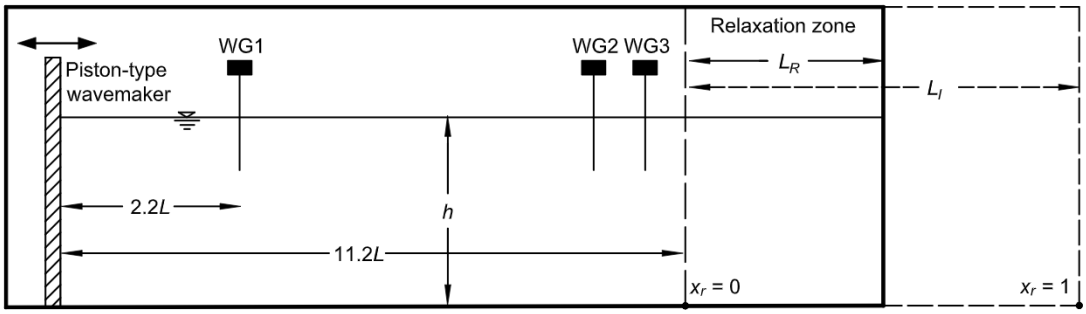

Fig. 3. Schematic showing the setup of the 2D NWT. WG: wave gauge.

for the smaller wave steepness ($kA = 0.071$) the reflection coefficient at $L_R/L_I = 0.5$ is slightly larger than that at $L_R/L_I = 1.0$, for the larger wave steepness ($kA = 0.142$) the situation reverses. This suggests a shift of the optimal ratio towards a larger number between 0.5 and 0.75 for the smaller wave steepness ($kA = 0.071$) and a smaller number between 0.4375 and 0.5 for the larger wave steepness ($kA = 0.142$), respectively. It is interesting to note that from the range $L_R/L_I = 0.125$ to 0.5, the modified relaxation method works the best for the largest wave steepness case under consideration (the reflection coefficients are always the smallest compared with the other two in a row), and again the situation reverses from the range $L_R/L_I = 0.75$ to 1.0. For the latter, this is consistent with the findings from other researchers who employ the regular relaxation method (see e.g. Jacobsen et al. (2012)), as the modified relaxation method becomes closer to the regular relaxation method. For the former, the reason is likely that as the same Courant number has been used, the computational time step of a larger wave steepness case is smaller than that of a smaller wave steepness case. So, within the same length of the relaxation zone where the relaxation function is flat and smooth, the incident wave as well as the reflected wave from the end of the relaxation zone are dissipated many more times in the larger wave steepness case; hence the smaller reflection coefficient.

3.1.2. *"Imaged" relaxation zone length*

The reflection coefficient run with three different "imaged" relaxation zone lengths are plotted in Fig. 4(a) as a function of the ratio L_R/L_I. Note that in these test cases the wave steepness is fixed at $kA = 0.106$. It can be seen from Fig. 4(a) that for all of the test cases the reflection coefficient decreases rapidly until $L_R/L_I = 0.5$. The optimal ratio for $L_I = 2.25L$ is approximately 0.5 as discussed in Section 3.1.1. The trend of the reflection coefficients for $L_I = 1.69L$ and $2.82L$, however, suggests a slight shift of the optimal ratio towards a larger

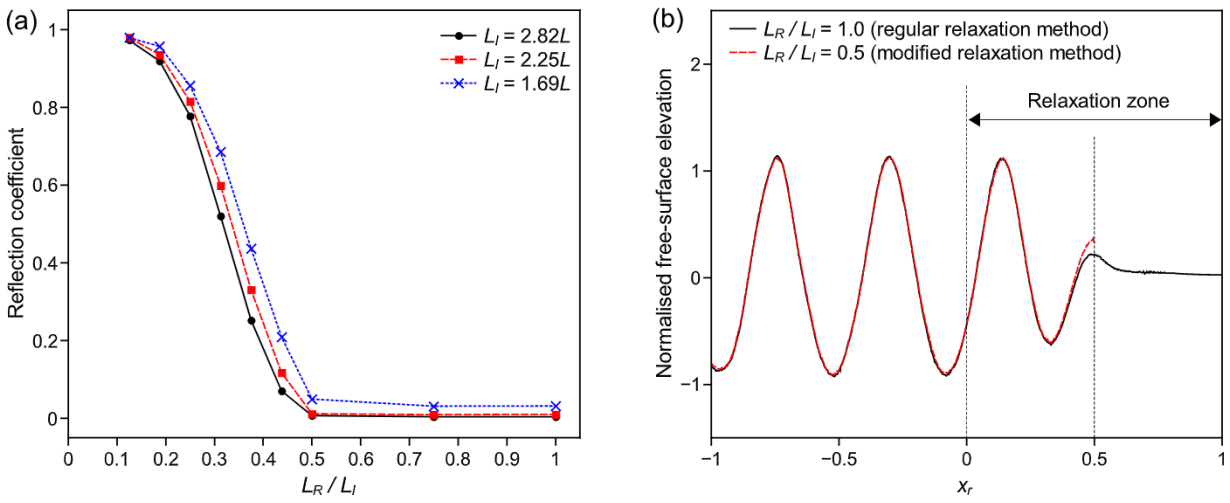

Fig. 4. Comparisons for (a) reflection coefficient run with three different "imaged" relaxation zone lengths with $kA = 0.106$; (b) snapshots of the free-surface elevations (normalised by the incident wave amplitude) run using the regular and the modified relaxation methods at the same times with $kA = 0.106$ and $L_I = 2.25L$.

Table 1
Reflection coefficients run with different wave steepnesses with $L_I = 2.25L$.

L_R/L_I	Reflection coefficient		
	$kA = 0.071$	$kA = 0.106$	$kA = 0.142$
0.1250	0.982	0.979	0.992
0.1875	0.942	0.936	0.921
0.2500	0.845	0.815	0.777
0.3125	0.647	0.599	0.547
0.3750	0.395	0.331	0.276
0.4375	0.165	0.117	0.080
0.5000	0.035	0.012	0.004
0.7500	0.007	0.009	0.015
1.0000	0.007	0.010	0.016

value and a smaller value than 0.5, respectively. In addition, as seen from Fig. 4(a) that at the same ratios L_R/L_I, larger L_I produces smaller reflection coefficient as expected. Also, it may be worth mentioning that from $L_R/L_I = 0.5$ to 1.0, all of the presented reflection coefficients are within 5%. Fig. 4(b) compares the snapshots of the free-surface elevations run using the regular and the modified relaxation methods ($L_R/L_I = 0.5$) at the same times for $L_I = 2.25L$. It can be seen that the free-surface elevations are almost identical, which further confirms the optimal ratio for $L_I = 2.25L$ mentioned above.

3.2. Solitary wave tests

In this section, solitary waves are used to test the modified relaxation method. The computations employ a 2D NWT similar to that used in the regular wave tests. The solitary wave is generated using a piston-type wave paddle, following the method proposed in Wu et al. (2016). Three different relative wave heights are tested: (a) $\varepsilon = 0.27$, (b) $\varepsilon = 0.33$ and (c) $\varepsilon = 0.40$, where $\varepsilon = a/h$, a is the crest height of the generated solitary wave and h is the water depth. In addition, three different "imaged" relaxation zone lengths are considered for the $\varepsilon = 0.40$ case: (a) $L_I = 2.03L$, (b) $L_I = 3.32L$ and (c) $L_I = 4.06L$, where L is the horizontal length scale over which the solitary wave has significant elevation. A uniform grid is used for all of the simulations with the number of grid cells ranging from approximately 13 to 20 along the wave heights and 700 to 570 across the wave lengths. The Courant number is fixed at 0.5.

Fig. 5 shows a typical series of snapshots at different times of the solitary wave propagating into a relaxation zone starting from $x/L = 0$ to $x/L = 4.06$. The results run with the regular relaxation method and the modified relaxation method (with $L_R/L_I = 0.5$) are plotted together for comparison. It can be seen from Fig. 5 that the majority of the wave energy is quickly dissipated in the first half portion of the relaxation zone as seen in the regular wave tests. Also, it is during this time period that, as seen from $t(g/h)^{1/2} = 47.1$, the main reflected waves are generated due to the existence of the relaxation zone. More interestingly, it is clearly seen that in this case the modified relaxation method with the ratio $L_R/L_I = 0.5$ produces results almost indistinguishable from those run with the regular relaxation method. This demonstrates the robustness of the suggested modified relaxation method for wave absorption.

Fig. 6 further presents the quantitative comparisons for the time histories of the free-surface elevation extracted at a location just in front of the relaxation zone. Both the results run with the regular relaxation method and the modified relaxation method are plotted, and note that for all of the cases with the modified relaxation method, $L_R/L_I = 0.5$. Fig. 6(a) compares the results run with different relative wave heights whilst the relaxation zone length is fixed at $3.32L$. The free-surface elevation η is normalised by the crest wave height a of the incident solitary wave. It is interesting to see that the relative height of the reflected wave (around $t(g/h)^{1/2} = 60$) is not significantly affected by the relative wave height of the incident solitary wave. Also, it can be seen that for all cases, the results run with the modified relaxation method match very well with those run with the regular relaxation method. This appears to be the same case for the results plotted in Fig. 6(b), which shows the comparison for the results run with different relaxation zone lengths L_I whilst the relative wave height ε is kept at 0.40. It is nevertheless seen in Fig. 6(b) that in these cases the relative height of the reflected wave decreases as the relaxation zone length increases, which is consistent with that found in the regular wave tests.

3.3. Focused wave tests

In this section, the modified relaxation method is applied to the focused wave generation presented in Chen et al. (2019). As reported in Chen et al. (2019), the focused wave is generated using the piston-type wave paddle through applying the Pierson–Moskowitz (PM) spectrum to the NewWave theory. The computations employ the 3D parallel version of the PIC model to establish the NWT. Despite being 3D, the setup of the NWT is similar to those used in the 2D tests, because the generated focused wave is unidirectional (propagating in the x-direction). The focused wave amplitude is set to 0.269 m and the water depth is fixed at 2.8 m. Along the x-direction, the distance between the wave paddle and the beginning of the relaxation zone is 7 m, and as in Chen et al. (2019), where the regular relaxation method is employed,

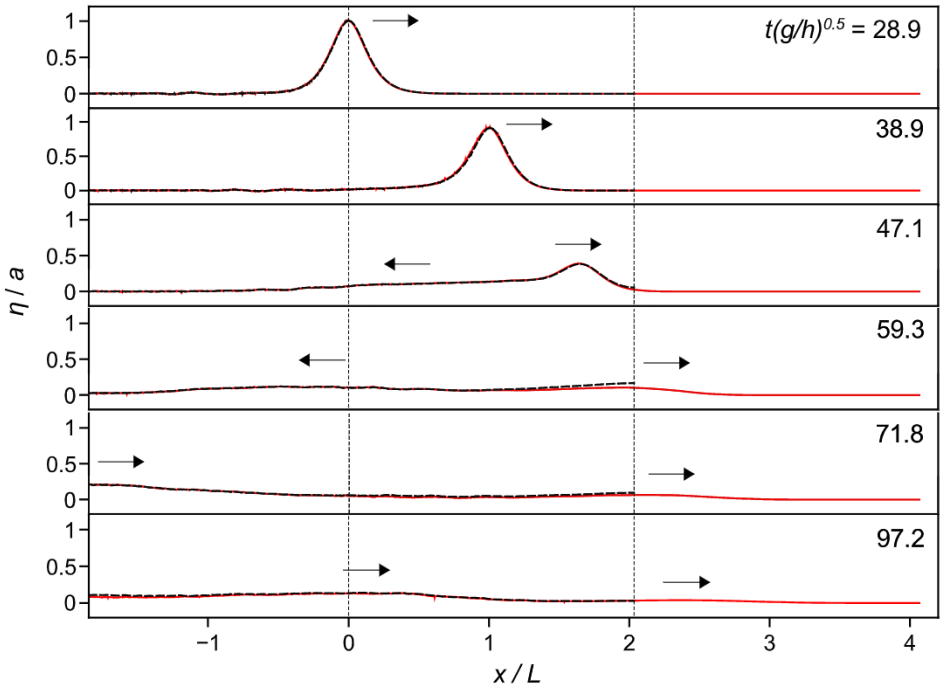

Fig. 5. Snapshots at various time instants of the solitary wave ($\varepsilon = 0.40$) propagating into a relaxation zone starting from $x/L = 0$. Red solid line: results run with the regular relaxation method ($L_I = 4.06L$); Black dashed line: results run with the modified relaxation method ($L_I = 4.06L$ and $L_R/L_I = 0.5$). The black arrows point at the propagation directions of the incident and the reflected waves.

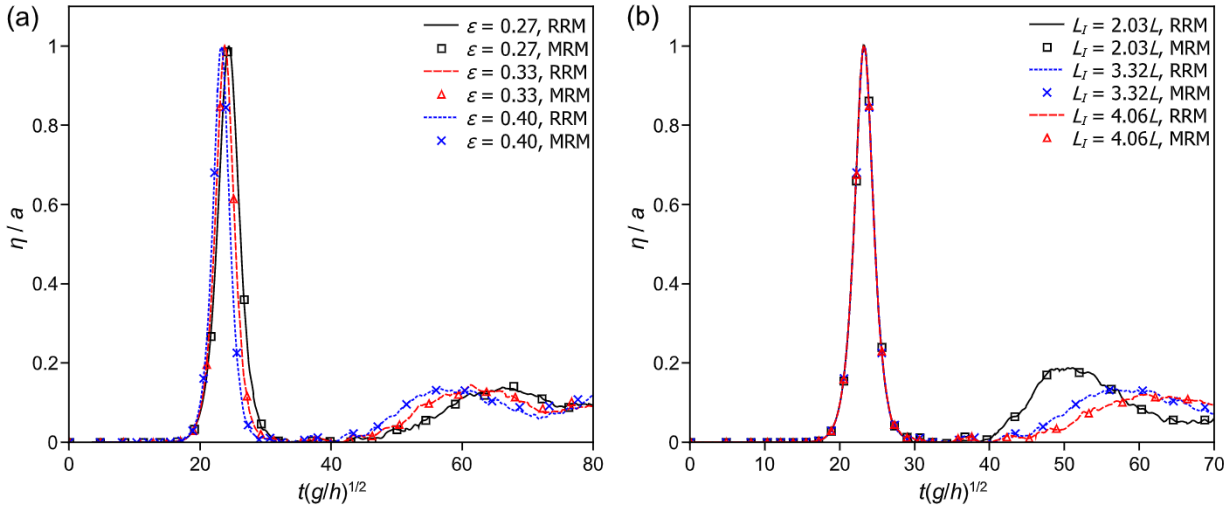

Fig. 6. Comparisons of the time histories of the free-surface elevation extracted at a location just in front of the relaxation zone: (a) results for different relative wave heights whilst L_I is fixed at $3.32L$; (b) results for different L_I whilst the relative wave height is fixed at $\varepsilon = 0.40$. RRM: regular relaxation method; MRM: modified relaxation method (for all cases $L_R/L_I = 0.5$).

L_I is set to $2L_p$, where $L_p = 11.27$ m is the wavelength corresponding to the peak frequency of the PM spectrum ($f_p = 0.356$ Hz). Four wave gauges are placed between the wave paddle and the relaxation zone along the centre line of the NWT in the x-direction to extract the generated focused wave elevations. In terms of the computation, a uniform grid size is employed following Chen et al. (2019), which are $\Delta x = \Delta y = \Delta z = 0.025$ m. As shown in Chen et al. (2019), this grid size enables the PIC model to well reproduce the focused wave compared to the measurements of a physical experiment. For full details of the setup of the NWT, the reader is referred to Chen et al. (2019). Here, the modified relaxation method with $L_R/L_I = 0.5$ is applied to this test case to demonstrate its performance.

Fig. 7 shows the comparison between the time histories extracted at the targeted focused location, which is 5.6 m from the wave paddle in the x-direction (correspondingly 1.4 m from the starting interface of the relaxation zone). Results run with the regular relaxation method and the modified relaxation method are plotted together for comparison. It can be seen that when reducing the original relaxation zone length to half and still using the regular relaxation method, discrepancies occur due to the reflection from the shortened relaxation zone. However, when reducing the original relaxation zone length to half but using the modified relaxation method instead, almost no extra wave reflection is produced. It should be noted that by using the modified relaxation method with half the relaxation zone, the total CPU time required for this test case has been reduced by approximately 27%.

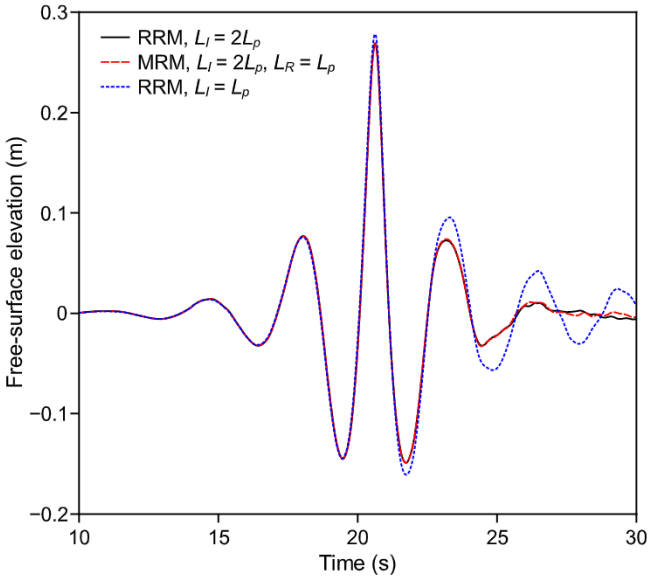

Fig. 7. Comparison between the time histories of the free-surface elevation extracted at the focused location. RRM: regular relaxation method; MRM: modified relaxation method.

4. Conclusions

In this short note, the effects of the relaxation approach on absorbing three type of waves (regular wave, solitary wave and focused wave) with different wave steepnesses and relaxation zone lengths are reported. In addition, a modification to the relaxation approach is suggested, based on the finding that the flat portion of the relaxation function is the most effective part in terms of wave absorption. The idea of the modification thus being that the length of the relaxation zone (that a regular relaxation method would use) can be reduced to keep just the flat portion of the relaxation function. The results show that the relaxation approach is effective on absorbing various waves in NWTs, given a sufficient length of the relaxation zone. This however can be computationally very expensive for CFD modelling especially when the wave length is large (e.g. solitary wave and focused wave). Furthermore, the results appear that the modified relaxation method tends to cut down the length of the relaxation zone by nearly 50% whilst still achieving similar performance to that of the regular relaxation method. In addition, based on the results of the regular wave tests, this amount increases slightly as the wave steepness increases or the relaxation zone length (that a regular relaxation method would use) increases. Whilst the results of this study, regarding the modified relaxation approach, are promising, the authors acknowledge that further testing is required before definitive conclusions can be drawn.

Acknowledgments

This work is supported by the UK–China joint project ResIn (EPSRC Grant No. EP/R007519/1). This work made use of the Balena High Performance Computing (HPC) Service at the University of Bath.

References

Armesto, J.A., Guanche, R., Iturrioz, A., Vidal, C., Losada, I.J., 2014. Identification of state-space coefficients for oscillating water columns using temporal series. Ocean Eng. 79, 43–49, URL http://www.sciencedirect.com/science/article/pii/S0029801814000225.

Chen, Q., 2017. Development of A Full Particle PIC Method for Simulating Nonlinear Wave-Structure Interaction (Ph.D. thesis). University of Bath.

Chen, Q., Kelly, D.M., Dimakopoulos, A.S., Zang, J., 2016a. Validation of the PICIN solver for 2D coastal flows. Coast. Eng. 112, 87–98, URL http://www.sciencedirect.com/science/article/pii/S0378383916300321.

Chen, Q., Zang, J., Dimakopoulos, A.S., Kelly, D.M., Williams, C.J., 2016b. A Cartesian cut cell based two-way strong fluid-solid coupling algorithm for 2D floating bodies. J. Fluids Struct. 62, 252–271, URL http://www.sciencedirect.com/science/article/pii/S0889974616000153.

Chen, Q., Zang, J., Kelly, D.M., Dimakopoulos, A.S., 2018. A 3D parallel Particle-In-Cell solver for wave interaction with vertical cylinders. Ocean Eng. 147, 165–180, URL http://www.sciencedirect.com/science/article/pii/S002980181730625X.

Chen, Q., Zang, J., Ning, D., Blenkinsopp, C., Gao, J., 2019. A 3D parallel particle-in-cell solver for extreme wave interaction with floating bodies. Ocean Eng. 179, 1–12, URL http://www.sciencedirect.com/science/article/pii/S002980181831504X.

Edwards, E., 2015. Simulating Water for Computer Graphics: Particle-In-Cell, Explicit Surfaces, and Discontinuous Galerkin (Ph.D. thesis). University of British Columbia, URL https://open.library.ubc.ca/collections/ubctheses/24/items/1.0223154.

Engsig-Karup, A.P., 2006. Unstructured Nodal DG-FEM Solution of High-Order Boussinesq-Type Equations (Ph.D. thesis). Technical University of Denmark.

Engsig-Karup, A.P., Hesthaven, J.S., Bingham, H.B., Madsen, P.A., 2006. Nodal DG-FEM solution of high-order Boussinesq-type equations. J. Engrg. Math. 56 (3), 351–370. http://dx.doi.org/10.1007/s10665-006-9064-z.

Finnegan, W., Goggins, J., 2012. Numerical simulation of linear water waves and wave–structure interaction. Ocean Eng. 43, 23–31, URL http://www.sciencedirect.com/science/article/pii/S0029801812000170.

Fuhrman, D.R., Madsen, P.A., Bingham, H.B., 2006. Numerical simulation of lowest-order short-crested wave instabilities. J. Fluid Mech. 563, 415–441.

Goda, Y., Suzuki, T., 1976. Estimation of incident and reflected waves in random wave experiments. Coast. Eng. Proc. 1 (15).

Harlow, F.H., 2004. Fluid dynamics in Group T-3 Los Alamos National Laboratory: (LA-UR-03-3852). J. Comput. Phys. 195 (2), 414–433, URL http://www.sciencedirect.com/science/article/pii/S0021999103005692.

Higuera, P., Lara, J.L., Losada, I.J., 2013. Realistic wave generation and active wave absorption for Navier-Stokes models: Application to OpenFOAM®. Coast. Eng. 71, 102–118, URL http://www.sciencedirect.com/science/article/pii/S0378383912001354.

Jacobsen, N.G., Fuhrman, D.R., Fredsøe, J., 2012. A wave generation toolbox for the open-source CFD library: OpenFoam®. Internat. J. Numer. Methods Fluids 70 (9), 1073–1088. http://dx.doi.org/10.1002/fld.2726.

Kamath, A., Bihs, H., Arntsen, Ø.A., 2015. Numerical modeling of power take-off damping in an oscillating water column device. Int. J. Mar. Energy 10, 1–16, URL http://www.sciencedirect.com/science/article/pii/S2214166915000028.

Kelly, D.M., Chen, Q., Zang, J., 2015. PICIN: A Particle–In–Cell solver for incompressible free surface flows with two-way fluid-solid coupling. SIAM J. Sci. Comput. 37 (3), B403–B424. http://dx.doi.org/10.1137/140976911.

Koo, W., Kim, M.-H., 2004. Freely floating-body simulation by a 2d fully nonlinear numerical wave tank. Ocean Eng. 31 (16), 2011–2046, URL http://www.sciencedirect.com/science/article/pii/S0029801804000976.

Madsen, P.A., Bingham, H.B., Schäffer, H.A., 2003. Boussinesq-type formulations for fully nonlinear and extremely dispersive water waves: derivation and analysis. Proc. R. Soc. Lond. Ser. A Math. Phys. Eng. Sci. 459 (2033), 1075–1104, URL http://rspa.royalsocietypublishing.org/content/459/2033/1075.

Mayer, S., Garapon, A., Sørensen, L.S., 1998. A fractional step method for unsteady free-surface flow with applications to non-linear wave dynamics. Internat. J. Numer. Methods Fluids 28 (2), 293–315, URL https://onlinelibrary.wiley.com/doi/abs/10.1002/%28SICI%291097-0363%2819980815%2928%3A2%3C293%3A%3AAID-FLD719%3E3.0.CO%3B2-1.

Palm, J., Eskilsson, C., Bergdahl, L., Bensow, R.E., 2018. Assessment of scale effects, viscous forces and induced drag on a point-absorbing wave energy converter by CFD simulations. J. Mar. Sci. Eng. 6 (4), URL http://www.mdpi.com/2077-1312/6/4/124.

Palm, J., Eskilsson, C., Paredes, G.M., Bergdahl, L., 2016. Coupled mooring analysis for floating wave energy converters using CFD: Formulation and validation. Int. J. Mar. Energy 16, 83–99, URL http://www.sciencedirect.com/science/article/pii/S2214166916300327.

Paulsen, B.T., Bredmose, H., Bingham, H.B., 2014. An efficient domain decomposition strategy for wave loads on surface piercing circular cylinders. Coast. Eng. 86, 57–76, URL http://www.sciencedirect.com/science/article/pii/S0378383914000155.

Ransley, E.J., Greaves, D., Raby, A., Simmonds, D., Hann, M., 2017. Survivability of wave energy converters using CFD. Renew. Energy 109, 235–247, URL http://www.sciencedirect.com/science/article/pii/S0960148117301799.

Windt, C., Davidson, J., Ringwood, J.V., 2018. High-fidelity numerical modelling of ocean wave energy systems: A review of computational fluid dynamics-based numerical wave tanks. Renew. Sustain. Energy Rev. 93, 610–630, URL http://www.sciencedirect.com/science/article/pii/S1364032118303629.

Wu, N.-J., Hsiao, S.-C., Chen, H.-H., Yang, R.-Y., 2016. The study on solitary waves generated by a piston-type wave maker. Ocean Eng. 117, 114–129, URL http://www.sciencedirect.com/science/article/pii/S0029801816300117.